Physica Medica 63 (2019) 25–34

Contents lists available at ScienceDirect

Physica Medica

journal homepage: www.elsevier.com/locate/ejmp

Original paper

Continuous generation of volumetric images during stereotactic body radiation therapy using periodic kV imaging and an external respiratory surrogate

M. Lafrenière[a,*], N. Mahadeo[a], J. Lewis[b], J. Rottmann[c], C.L. Williams[a]

[a] Brigham and Women's Hospital, Dana-Farber Cancer Institute, Harvard Medical School, 75 Francis St, Boston, MA 02215, USA
[b] University of California, Los Angeles, CA 90095, USA
[c] Paul Scherrer Institute, Forschungsstrasse 111, 5232 Villigen, Switzerland

ARTICLE INFO

In memory of Guillaume Barlet

Keywords:
Respiratory motion modeling
Continuous volumetric image generation
Deformable image registration (DIR)
Principal component analysis (PCA)
External respiratory surrogate

ABSTRACT

We present a technique for continuous generation of volumetric images during SBRT using periodic kV imaging and an external respiratory surrogate signal to drive a patient-specific PCA motion model. Using the on-board imager, kV radiographs are acquired every 3 s and used to fit the parameters of a motion model so that it matches observed changes in internal patient anatomy. A multi-dimensional correlation model is established between the motion model parameters and the external surrogate position and velocity, enabling volumetric image reconstruction between kV imaging time points. Performance of the algorithm was evaluated using 10 realistic e**X**tended **CA**rdiac-**T**orso (XCAT) digital phantoms including 3D anatomical respiratory deformation programmed with 3D tumor positions measured with orthogonal kV imaging of implanted fiducial gold markers. The clinically measured ground truth 3D tumor positions provided a dataset with realistic breathing irregularities, and the combination of periodic on-board kV imaging with recorded external respiratory surrogate signal was used for correlation modeling to account for any changes in internal-external correlation. The three-dimensional tumor positions are reconstructed with an average root mean square error (RMSE) of 1.47 mm, and an average 95th percentile 3D positional error of 2.80 mm compared with the clinically measured ground truth 3D tumor positions. This technique enables continuous 3D anatomical image generation based on periodic kV imaging of internal anatomy without the additional dose of continuous kV imaging. The 3D anatomical images produced using this method can be used for treatment verification and delivered dose computation in the presence of irregular respiratory motion.

1. Introduction

Respiratory motion is an outstanding challenge for radiation therapy treatments of many thoracic and abdominal malignancies. This motion may result in organ displacements of several centimeters, particularly in the superior-inferior (SI) direction [1–3]. The respiratory motion is three-dimensional and non-rigid, affecting both the target lesion(s) as well as adjacent organs at risk, potentially causing deviations in the planned dose (target underdosage and increased dose to normal tissues) [4,1,2,5,6].

In current standard clinical practice, accounting for organ motion relies on the use of 4DCT [7,8] to define an internal target volume that encompasses the target motion. In standard 4DCT acquisition protocols, the imaging represents just one or two respiratory cycles in each region of the patient anatomy. This inherently presents a limited view of the patient's breathing pattern as it does not reflect any breath-to-breath changes in motion. This can lead to substantial uncertainties in the internal target volume derived from a 4DCT dataset [9–12]. Moreover, 4DCT images obtained during pre-treatment simulation may not represent internal patient anatomy and organ motion at the time of treatment, as the patient's breathing pattern may change in the intervening time [13,14]. Even with modern techniques such as using 4DCT during simulation, using breathing coaching or the ABC method, there are still residual uncertainties in the location of the target and normal tissue due to day-to-day changes in a patient's breathing pattern. The impact of these day-to-day changes on the delivered dose is not well known, and may lead to deviations between the planned and the delivered dose. Generating continuous 3D images would allow to assess these changes and to potentially re-calculate the delivered dose, to improve the accuracy and safety of SBRT.

* Corresponding author at: Brigham and Women's Hospital, Dana-Farber Cancer Institute, Harvard Medical School, 75 Francis St, ASBI-L2, Boston, MA 02215, USA.
E-mail addresses: matthieu_lafreniere@dfci.harvard.edu (M. Lafrenière), cwilliams@bwh.harvard.edu (C.L. Williams).

https://doi.org/10.1016/j.ejmp.2019.05.012
Received 22 March 2019; Received in revised form 26 April 2019; Accepted 18 May 2019
Available online 25 May 2019

Respiratory motion modeling techniques can be used to overcome some of the limitations of traditional 4DCT-based techniques, enabling improved 3D localization of target lesions and surrounding normal tissues [15–20]. Often, these patient-specific motion-models are created with information available prior to radiotherapy treatment, such as 4DCT [21,22,20,23], 4DCBCT [24,25], or an external surrogate signal [26]. Deformable image registration (DIR) can be performed between the 3D images of each respiratory phase to produce a set of 3D displacement vector fields (DVFs) that describe the respiratory motion in these scans.

A simplified model of the motion-induced deformations can be created by using a dimensionality-reduction technique, such as PCA, which allows the full DVF to be described as a linear combination of a small subset of vector fields. The entire 3D representation of a patient's anatomy at an arbitrary respiratory state can then be generated using only a small number of model parameters. Other information, such as lung tidal volume and airflow [23], or an external respiratory surrogate [26–29,19] can also be incorporated in the model.

3D fluoroscopic image generation is a technique that uses a patient-specific respiratory motion model in combination with 2D X-ray projection images acquired during treatment to reconstruct a full 3D volume [14]. Parameters of the motion model are determined using an iterative optimization procedure in which a digitally reconstructed radiograph (DRR) of the modeled patient anatomy is compared with the acquired image, and the model parameters are then adjusted for an optimal match.

Previous motion modeling-based approaches have demonstrated that kV or MV images [30,24,25,31,14], as well as external surrogate signals [26,32], can be used independently to generate volumetric images. However, these techniques have limitations that can pose challenges for clinical implementation. For kV image-based techniques, the image acquisition frame rate is impacted by the potential for excess imaging dose (continuous fluoroscopy can add up to 1.2 Gy over a treatment course [33–35]), as well as machine constraints (e.g. the Varian TrueBeam platform used in our clinic limits in-treatment kV imaging to a rate of 1/3 Hz in clinical mode), which may result in images being acquired too infrequently to fully capture the motion during each breath. The use of MV portal images is also limited due to the small and complex apertures used with modulated treatments as well as reduced soft-tissue contrast. For external surrogate-based techniques, the correlation between the surrogate signal and internal patient anatomy can change over time [36–38].

Prior studies have shown that it is possible to track tumor motion using orthogonal kV imaging of implanted fiducial gold markers and with an external surrogate infrared signal to assess internal-external anatomy correlation [39–45]. However, these techniques only track the motion of the fiducial markers, and do not capture the full three-dimensional motion, which may include relative motion between the tumor and nearby organs at risk. Furthermore, many clinical accelerators often do not have fixed orthogonal X-ray systems.

We present a technique that combines periodic triggered kV images with an external respiratory surrogate to drive a patient-specific motion model built from a pre-treatment 4DCT scan. This method is novel in that it combines image-derived model fitting with a continuous external surrogate signal, providing the capability to generate continuous volumetric images based on kV images of internal anatomy changes while at the same time requiring only limited kV imaging. This technique addresses many limitations of previous motion modeling techniques and enables high time-resolution 3D anatomical image generation using information that is available on current clinical treatment machines and often already acquired as part of current clinical treatments.

2. Methods and materials

2.1. Technique overview

This technique extends prior work that generates 3D anatomical images based on single kV radiographs [14,31] or external surrogate signals [26], and establishes a framework that uses information from both approaches through a correlation model.

It is designed to rely on capabilities that are already present in or integrated with many current clinical treatment machines: an on-board kV imaging source and panel, and an external respiratory surrogate.

A patient would be set up for treatment according to clinical standard of care, with the addition of a respiratory monitoring device such as an abdominal marker block (e.g. as in the RPM system [1,46–51]) or spirometry device [23,52–55]. Additionally, during treatment the kV imaging panel would be deployed and would acquire kV images every 3 s (this is the current maximum frame rate of the in-treatment kV image functionality in clinical mode on the Varian TrueBeam accelerators used in our clinic). The information from these modalities will then be combined with a motion model from a treatment planning 4DCT (or potentially a pre-treatment 4DCBCT) to enable volumetric image generation.

2.2. Modified digital XCAT phantom with realistic breathing from clinically measured patient data

The overall accuracy of a time-varying volumetric anatomical image generation technique can be difficult to assess with clinically acquired data due to the lack of a ground truth volumetric image to compare the generated volumetric image against. To address this issue, we use the hybrid digital e**X**tended **CA**rdiac-**T**orso (XCAT) phantom [56–58] seen in Fig 1. This phantom incorporates realistic anatomy [59] for which a ground truth is unambiguously defined from clinical tumor position measurements, and also allows for customized irregular breathing profiles [60,61]. This technique has been developed and used previously in our group [14,26,31,25,24,62,63], and has proved useful in quantitatively assessing the accuracy of the 4D anatomical image generation over a variety of patient-simulated conditions.

The tumor motion trajectories that were used to generate the XCAT phantoms were acquired with the Mitsubishi Real Time Radiation Therapy (RTRT) system at the Radiation Oncology Clinic at the Nippon Telegraph and Telephone Company Hospital in Sapporo, Hokkaido, Japan [36–38,64,65]. A fluoroscopic X-ray system was used to obtain stereoscopic images to localize 1.5 mm gold fiducial markers implanted in lung tumors of patients receiving radiotherapy. Volumetric digital XCAT phantoms were generated for each measured 3D tumor motion trace. The simulated tumors were modeled as 2 cm diameter spheres whose centroid moves in accordance with the tumor motion measured using the RTRT system. The breathing motion of the XCAT phantom is

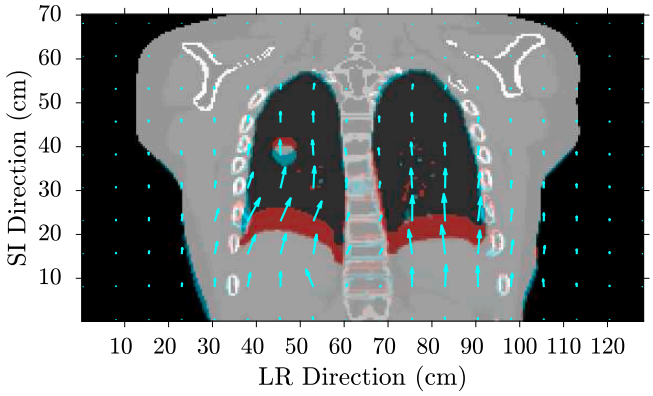

Fig. 1. Example digital XCAT phantom reference coronal slice image (red) overlayed with a reconstructed coronal slice image from an inhale respiratory phase (cyan) of phantom #5, showing the tumor and diaphragm moving inferiorly. The reconstructed displacement vector field between the reference and reconstructed image is also shown (cyan arrows). (For interpretation of the references to colour in this figure legend, the reader is referred to the web version of this article.)

controlled by the diaphragm displacement and anterior motion of the ribs, and these parameters were varied to reproduce the observed 3D tumor motion. The remainder of the anatomy is moved and displaced according to the deformation model within the XCAT software, which can be nonlinear.

In addition to the stereoscopically-acquired tumor positions, the RTRT system also included an external respiratory surrogate (the Anzai 733 V external respiratory surrogate laser-based system [66,38]) that reported the position of the patient's abdomen at a rate of 30 Hz [64,65]. The synthetic XCAT images produced in this study are thus independent from the external surrogate information used to build the correlation model and being drawn from the RTRT dataset.

Ten XCAT phantom sets were generated from 9 separate patients (two separate datasets came from the same patient). An open source graphical user interface software was used to facilitate the creation of digital XCAT phantoms based on tumor positions clinically recorded with the RTRT system [67]. Phantoms were created with an intrinsic resolution of 2 mm in the left-right (LR) and anterior-posterior (AP) directions, and 2.5 mm in the superior-inferior (SI) direction. The total number of voxels per image is $256 \times 256 \times 140 = 9,175,040$ (LR, AP, SI). The XCAT images were produced every 0.2 s, and for each patient the entire available respiratory trace was used, which varied between 46.7 s and 292.0 s.

A training 4DCT dataset consisting of 10 images approximately distributed over the first breathing cycle in the respiratory trace was produced for each XCAT dataset, replicating the information that would be available to train a motion model from clinical 4DCT images (empty cyan triangles in Fig. 2). These "4DCT" XCAT images are spaced every 0.4 s for a total of 4 s, similarly to previous studies on 4DCT motion modeling using the XCAT phantom [68,14,31].

2.3. Volumetric image generation

2.3.1. PCA based respiratory motion model

Each respiratory phase of the digital XCAT phantom training 4DCT dataset was deformably registered to a peak-exhale reference image from the same dataset using a graphics processing unit (GPU) accelerated double force demons algorithm [69] with the α parameter fixed to 2.0. A patient-specific motion-model was then constructed by performing PCA on the DVFs obtained with the registration, and retaining only the most important eigenvectors. DVFs describing the respiratory motion can typically be well represented by a linear combination of 2–3 PCA eigenvectors [26,31,14,70,22,68,28,71,72,17,19,73]:

$$\mathbf{DVF} = \overline{\mathbf{DVF}} + \sum_{n=1}^{N} w_n(t)\mathbf{u_n} \tag{1}$$

where $\overline{\mathbf{DVF}}$ is the mean **DVF**, $\mathbf{u_n}$ is the n^{th} basis eigenvector, $w_n(t)$ is the time dependent weighting coefficient (also called PCA eigenvalue, or PCA weight) of the n^{th} PCA mode, and N is the total number of PCA modes that are used for motion modeling. Three PCA weighting coefficients were used for each XCAT dataset to build the respiratory motion models for this work.

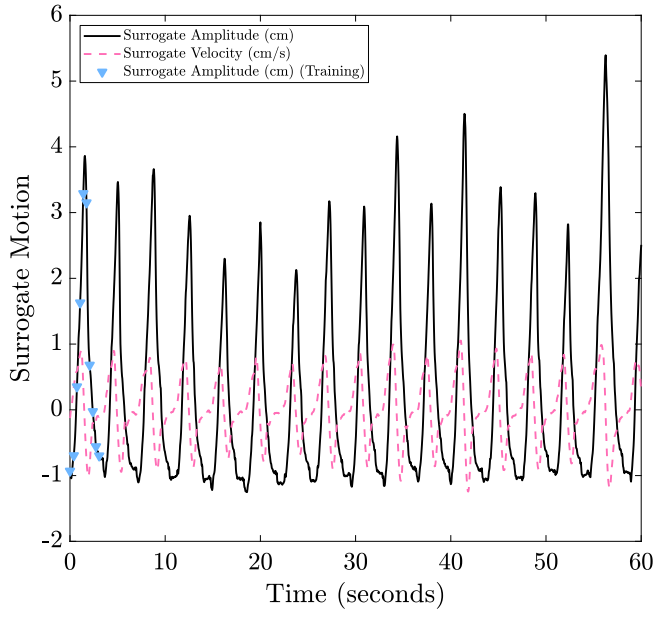

Fig. 2. First 60 s of the respiratory trace from phantom #5 showing the external surrogate amplitude (plain black line), the surrogate velocity (dashed magenta line) and the time points chosen for generating the simulated 4DCT training phantoms (cyan triangles) used for creating the motion model. (For interpretation of the references to colour in this figure legend, the reader is referred to the web version of this article.)

2.3.2. Optimization-based 3D image generation

A 3D image can be produced from a single 2D X-ray image by using a forward iterative reconstruction (FIR) process to optimize the weights ($w_n(t)$) in the PCA respiratory motion model so that the projection of the deformed reference CT image matches the observed X-ray image. This deformed reference CT image ($\mathbf{f}$) is created by deforming the reference image ($\mathbf{f_0}$), with a displacement vector field ($\mathbf{DVF}(w)$) determined by the PCA weights. A simulated X-ray image ($\mathbf{P}\cdot\mathbf{f}$) can be produced by applying a projection matrix ($\mathbf{P}$) to the deformed reference CT image ($\mathbf{f}$). An iterative minimization procedure is then performed to match the simulated X-ray image ($\mathbf{P}\cdot\mathbf{f}$) and the observed X-ray image ($\mathbf{x}$) acquired during treatment delivery:

$$\min_{w} J(w) = \min_{w} \left\| \mathbf{P}\cdot\mathbf{f}(\mathbf{DVF}(w), \mathbf{f_0}) - \lambda\cdot\mathbf{x} \right\|_2^2, \tag{2}$$

where λ is a parameter defining the relative pixel intensity between simulated X-ray projections and acquired X-ray images, and $J(w)$ is a cost function representing the L2-norm (squared least squares) error between the simulated and acquired X-ray image. A version of gradient descent is used to minimize the cost function $J(w)$ (Eq. 2). A detailed description of the PCA coefficients optimization can be found in the work of Li et al. [68,71]. The resulting deformed reference CT image ($\mathbf{f}$) corresponds to the optimized estimate of the 3D anatomy at the time of the X-ray acquisition. A schematic representation of this process is shown in Fig. 3. This process is implemented in a GPU-accelerated framework so that it can be performed in real time.

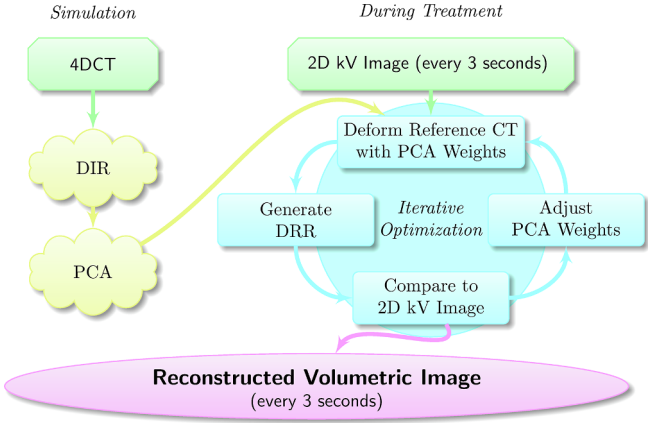

Fig. 3. Forward iterative reconstruction (FIR) procedure for estimating time-varying volumetric images from single X-ray projections. In this work, a method was developed to use an external respiratory surrogate to generate volumetric images in the 3-s time interval elapsed between each acquired kV image.

2.3.3. Continuous volumetric image generation with an external surrogate respiratory trace

During radiotherapy treatments, it may not be possible or desirable to acquire kV images continuously due to imaging dose or machine limitations. Thus, the framework presented in Fig. 3 is extended to continuously generate 3D images in the time interval between each kV image acquisition. To accomplish this, we use the information provided by an external respiratory surrogate to estimate the motion model PCA weights during the image acquisition 3 s time interval. This is a non-invasive, non-ionizing modality that provides the amplitude of a patient's abdominal motion with high time resolution (30 Hz).

A linear correlation model is developed between the PCA weights, and the displacement and velocity of the surrogate signal. These surrogate characteristics have been shown to be complementary in characterizing respiratory motion [74,26]. For each kV image acquisition, the weight of each PCA mode, w_n, is determined by the procedure described in Section 2.3.2, and the correlation model is established:

$$w_n(t) = c_n + f_n a(t) + g_n \dot{a}(t) \tag{3}$$

where $a(t)$ is the amplitude of the external surrogate signal, and $\dot{a}(t)$ is its velocity. The parameters c_n, f_n and g_n are specific to each PCA mode of each patient's motion. The linear relationship between the first principal component (w_1) and the external surrogate amplitude and velocity ($a(t)$ and $\dot{a}(t)$) is shown in Fig. 4, and is represented by the linear fitting surface. The first PCA component has the most importance and primarily drives the motion model, as seen in Figs. 5–7. Correlation model generation is performed on a per-fraction basis because of potential inter-fraction changes in the correlation between internal and external anatomy [36–38].

PCA weights periodically reconstructed with the FIR process and PCA weights continuously generated with the correlation model are shown as a function of the external surrogate amplitude for phantom dataset #5 in Fig. 5. The same PCA weights, but as a function of the external surrogate velocity, are shown in Fig. 6. Finally, the PCA weights as a function of time are shown in Fig. 7.

2.4. Evaluation criteria

The tumor localization error is evaluated with the 95th percentile and the RMSE between the tumor centroid location in the reconstructed volumetric images and the ground truth volumetric images. The tumor localization error is estimated in the LR, AP, and SI directions, as well as an absolute 3D positional difference, which provides a geometric measure of the reconstruction accuracy.

As a benchmark for comparison, the FIR process was also performed every 0.2 s, to simulate continuous kV fluoroscopy for generating motion model reconstructions. Comparing these results to the correlation model (which uses imaging every 3 s) allows the accuracy of the correlation method to be assessed in the context of the overall performance of the image-based motion modeling techniques.

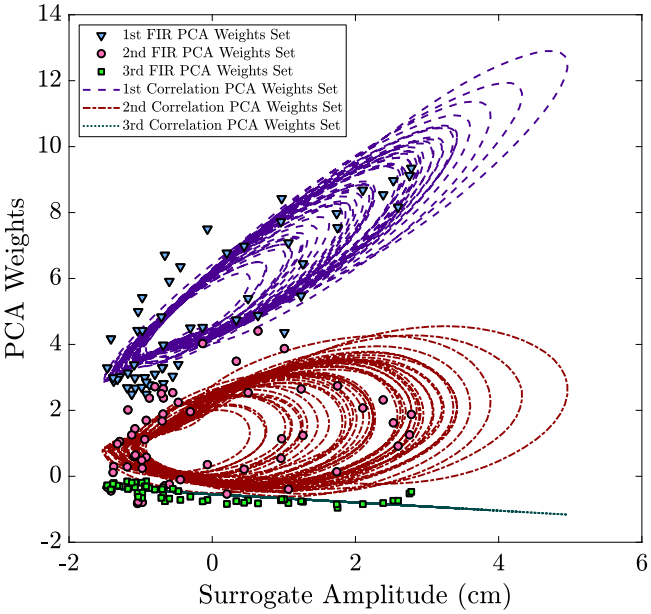

Fig. 5. Three PCA weights sets created from kV images (markers) and generated with the correlation model (lines) as a function of the external surrogate amplitude for phantom dataset #5.

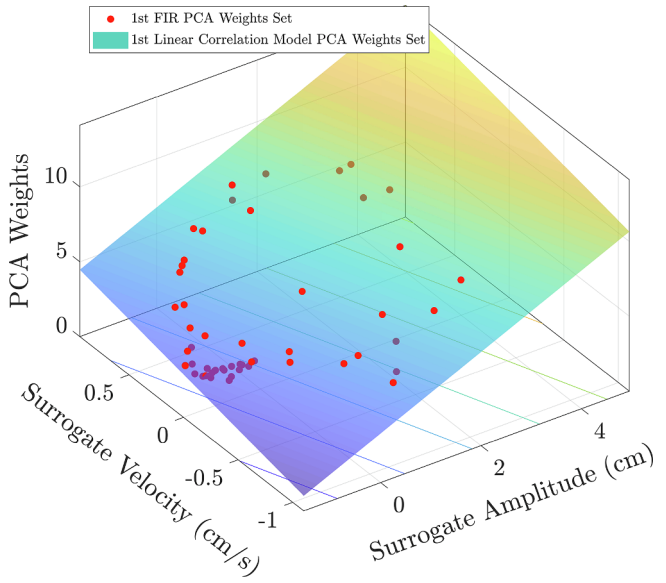

Fig. 4. The weights of the first principal component of phantom dataset #5 plotted as a function of the external surrogate amplitude and velocity. The linear correlation model is represented by the fitting surface.

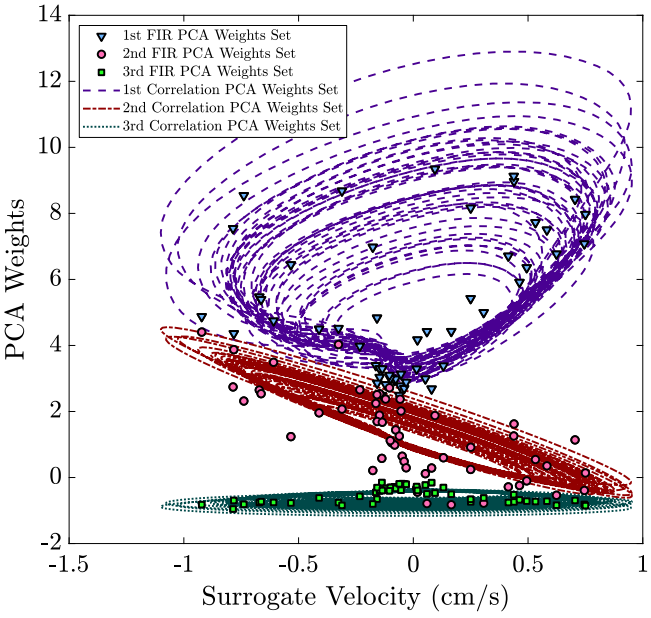

Fig. 6. Three PCA weights sets created from kV images (markers) and generated with the correlation model (lines) as a function of the external surrogate velocity for phantom dataset #5.

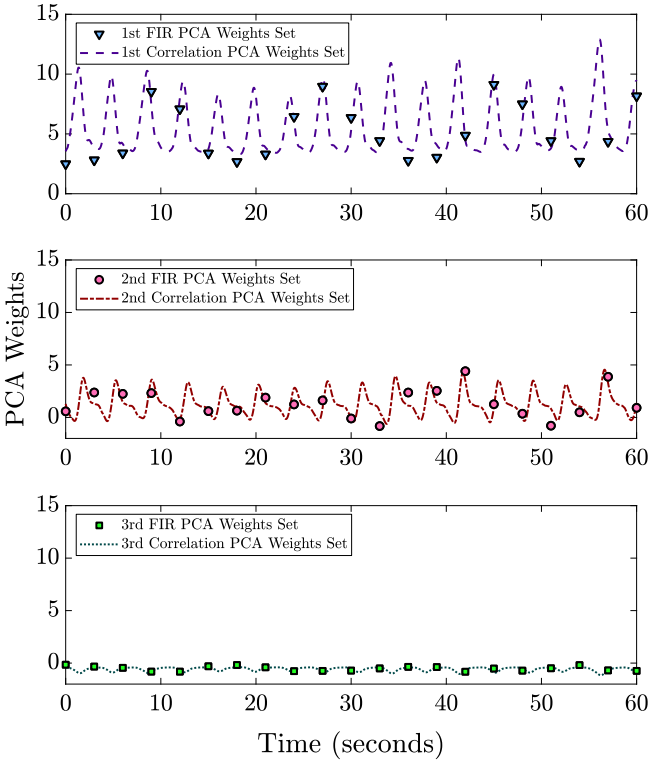

Fig. 7. Three PCA weights sets created from kV images (markers) and generated with the correlation model (lines) as a function of time (phantom dataset #5). The simulated kV image rate used in the motion model for reconstruction is 1/3 Hz. The first PCA component has the dominant motion contribution.

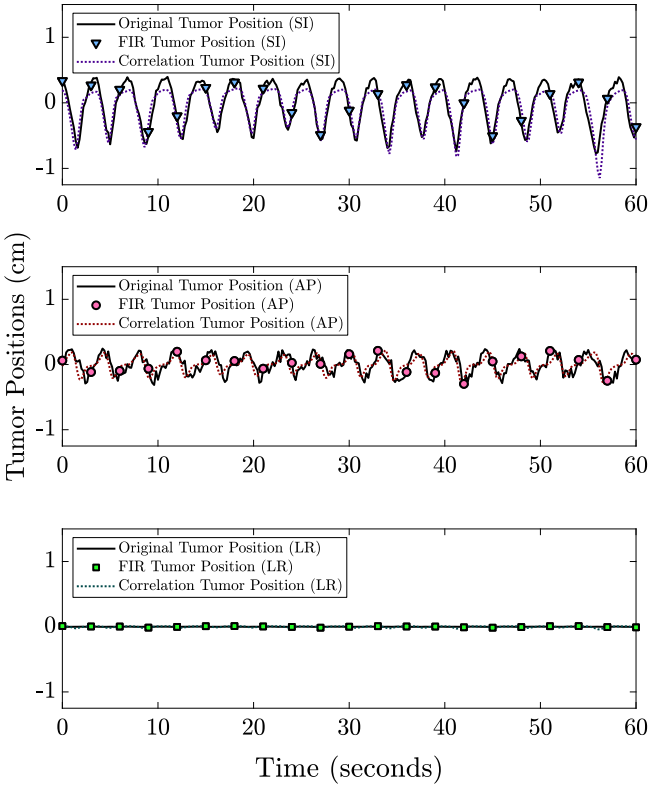

Fig. 8. Ground truth tumor positions in the LR, AP and SI directions (plain black lines), alongside those created by the FIR algorithm (markers) and by the correlation model (non-continuous colored lines) (phantom dataset #5). The simulated kV image rate used in the motion model for reconstruction is 1/3 Hz. The main contribution to respiratory motion comes from the SI direction.

3. Results

The correlation method's performance was evaluated by comparing the position of the tumor centroid in reconstructed images to the tumor centroid position in the ground truth phantom images for each dataset. Simulated kV images were computed every 3 s to match the acquisition rate of current radiotherapy clinical systems. The image-based fitting procedure described in Section 2.3.2 was used to generate periodic PCA weights, and continuous correlation model PCA weights were determined using the full external surrogate respiratory trace.

Using the correlation model, three-dimensional reconstructions were computed every 0.2 s over the entire respiratory trace duration. The average trace length was 155.8 s long (ranging from 46.7 to 292.0 s). The motion in the datasets was primarily in the SI direction, and the average 3D motion amplitude was 1.7 cm. The ground truth 3D tumor positions compared with the reconstructed 3D tumor positions for a representative respiratory trace are shown in Fig. 8. (See Fig. 9).

The accuracy of the 3D tumor positions and the 3D images reconstructed with FIR and the correlation model (COR) for each phantom dataset is summarized in Table 1. The average 95th percentile 3D error between correlation model-generated volumetric images and ground truth volumetric images was 2.80 mm, and the RMSE was 1.47 mm (results averaged over 10 different phantom datasets). On average, tumor positions reconstructed using the correlation model method were within 3 mm of the ground truth position 94.6% of the time, and below 5 mm 99.1% of the time. A plot of the cumulative 3D differences in tumor location between the ground truth and the correlation model for all generated images from dataset #5 is shown in Fig. 10. Comparison of the full volumetric ground truth and correlation model generated images gives a NRMSE of 97.83% (refer to Table 1).

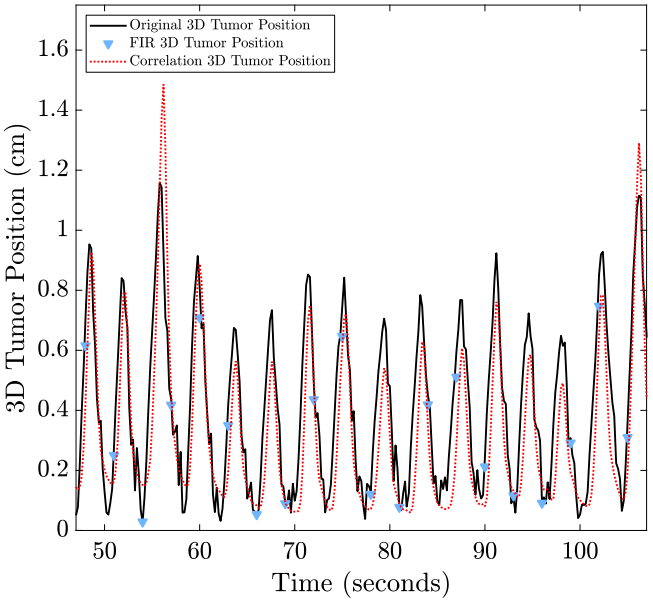

Fig. 9. The ground truth three dimensional tumor positions (plain black curve) is displayed alongside the correlation model reconstructed 3D tumor positions (dashed red curve), and the positions determined from performing the FIR process on 1/3 Hz kV images (cyan triangles) (phantom dataset #5), illustrating the ability of the technique to reconstruct motion with high time resolution, even in the presence of irregular breathing.

Table 1
Three dimensional tumor positions over an average respiratory trace duration of 155.8 s are reconstructed with a 95th percentile of 1.58 mm with FIR, and 2.80 mm with the correlation model (COR) (averaged over 10 datasets). The RMSE between ground truth and FIR generated volumetric images is 0.94 mm with FIR, and the RMSE between ground truth and the correlation (COR) generated volumetric images is 1.47 mm (averaged over 10 datasets). The voxel by voxel intensity volumetric image comparison yields a normalized root mean squared error of 98.16% with FIR, and a NRMSE of 97.83% with the correlation model (COR) (averaged over 10 datasets).

XCAT Dataset	Length (seconds)	3D tumor position reconstruction under 1 mm (%)		3D tumor position reconstruction under 3 mm (%)		3D tumor position reconstruction under 5 mm (%)		3D tumor position reconstruction 95^{th}p (mm)		3D tumor position reconstruction RMSE (mm)		3D image comparison NRMSE (%)	
		FIR	COR	FIR	COR	FIR	COR	FIR	COR	FIR	COR	FIR	COR
1	61.8	59.9	36.6	94.2	83.2	96.8	93.5	3.21	6.31	1.46	2.64	98.29	97.96
2	75.6	93.9	65.5	98.4	96.0	99.2	98.1	1.11	2.75	0.99	1.87	98.73	98.38
3	46.7	75.1	76.4	100	99.1	100	100	1.51	2.22	0.85	0.96	96.87	95.96
4	141.3	100	98.0	100	100	100	100	0.35	0.86	0.21	0.45	98.73	98.62
5	161.4	95.7	54.6	100	97.6	100	99.8	0.97	2.62	0.54	1.36	98.22	97.65
6	141.3	100	61.3	100	98.9	100	100	0.48	2.29	0.29	1.16	98.65	98.56
7	169.1	49.9	45.3	94.7	100	100	100	2.02	2.39	1.16	1.39	98.39	98.37
8	223.8	59.1	65.9	100	99.5	100	100	1.91	2.12	1.09	1.07	97.90	97.47
9	245.0	13.5	26.8	97.4	73.8	100	100	2.93	3.90	2.13	2.40	97.97	97.79
10	292.0	71.1	48.3	100	98.4	100	100	1.35	2.50	0.80	1.38	97.82	97.48
Average	155.8	71.8	57.9	98.5	94.6	99.6	99.1	1.58	2.80	0.94	1.47	98.16	97.83

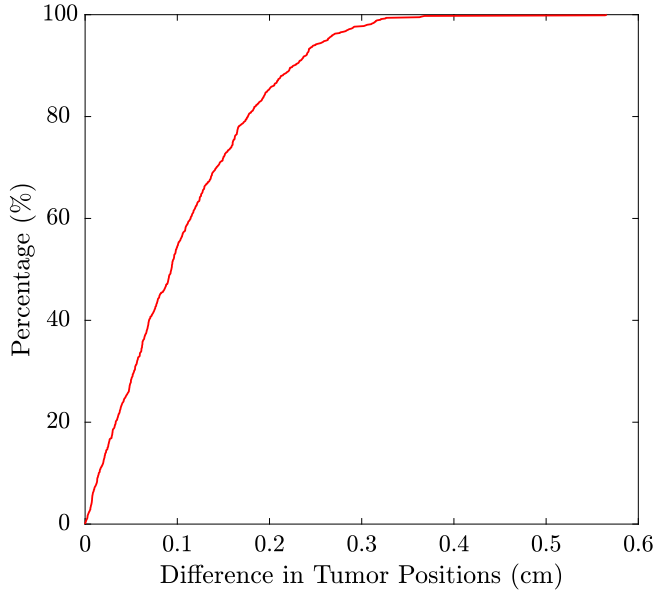

Fig. 10. Cumulative difference between the ground truth 3D tumor positions and the 3D tumor positions reconstructed using the correlation model (phantom dataset #5). For this dataset, the 95^{th} percentile is 2.62 mm, and the RMSE is 1.36 mm. When averaged over all datasets, the 3D tumor position difference is below 2.80 mm for 95% of the data, and below 3 mm for 94.6% of the data.

A baseline accuracy for the image-based reconstruction method was assessed by performing the FIR process every 0.2 s to simulate near-continuous kV acquisition. This kV-based motion modeling technique was characterized by an average 95**th** percentile accuracy of 1.58 mm and an average RMSE of 0.94 mm for the three dimensional tumor position reconstruction. This shows that the tumor position reconstruction obtained with the FIR process is better than a millimeter. When comparing the ground truth and FIR generated volumetric images, the NRMSE is 98.2% (refer to Table 1).

4. Discussion

This method provides a new way to continuously generate 3D images throughout a radiotherapy treatment by establishing a correlation model between motion model PCA weights determined from kV images (using information from the internal anatomy) and the amplitude and velocity of an external respiratory surrogate signal, which inherently takes into account any changes in the correlation between the internal and the external anatomy. This technique uses data that are often already available during treatments on conventional linear accelerators, and obviates the need to capture kV images at a high frame rate in order to accurately perform motion model-based 3D anatomical image reconstruction.

Several techniques to track the tumor position under respiratory motion using fluoroscopic kV imaging have been developed [75–80,35,81,82], however the additional dose due to the continuous kV image acquisition may be undesirable. The technique presented in this work enables anatomic tracking using only periodic kV imaging. Furthermore, by fitting a full 3D motion model (rather than tracking individual points), the entire 3D patient anatomy can be reconstructed, enabling delivered dose calculation.

The correlation model used in this work differs from other techniques that have used internal-external correlation [83–88,37,43,44,89–91] in that it relates both the surrogate amplitude and velocity to the PCA deformation vector fields in the motion model (as opposed to correlating surrogate amplitude and target position). Consequently this technique tracks tumor positions and also determines the deformation of the entire patient's anatomy, including nearby organs at risk. The model can also be updated based on observed internal anatomy as more kV images are acquired. Additionally, as this technique uses information from the entire kV image (as opposed to just the tumor region), it does not suffer from limitations on tumor size or distance to other nearby structures that can often confound image-based tumor tracking techniques [92]. As the *cine* 3D images produced by this method are generated from deformations of a reference 4DCT planning image, they are inherently co-registered with known deformations. The DVFs produced by the motion model can then be used to calculate and accumulate the delivered dose to the patient, providing a mechanism to compute the full delivered dose in the presence of respiratory motion during treatment.

The 3D tumor positions are reconstructed with an average RMSE of 1.47 mm, which compares favorably with other similar tracking methods that use both images and external surrogates (e.g. the Xsight Lung Tracking System, which has a precision of 1.5 mm to 4 mm [40,41,93,43–45]). Performing volumetric image reconstruction with the FIR process using high frame rate kV images (0.2 s interval) yields an average RMSE of 0.94 mm in the tumor position reconstruction. Comparing to the results of the correlation model with a 3-s imaging

interval shows that although the accuracy of the reconstruction decreases, the overall performance degradation (0.53 mm in the RMSE) is small compared to typical respiratory motion amplitudes. Voxelwise intensity comparison of both the FIR-generated and correlation model-generated volumetric images to the ground truth images yields a similar NRMSE, indicating good agreement between the methods in regions outside of the tumor.

The use of XCAT phantoms enabled a detailed analysis of the full 3D accuracy of this technique. Although the phantoms used in this study match clinically observed respiratory patterns, the internal anatomic details of the phantom are not fully representative of a real patient. This could impact the performance of the deformable image registration as well as the fitting of the PCA weights from kV images. Additionally, physical effects such as scatter or imaging artifacts are not included in the image projection process. A full validation of this technique is currently undergoing with clinically acquired 4DCT and kV images. However, the ground truth comparison provided by this phantom study provides essential data to evaluate the accuracy of our technique and will be required to better understand results from the patient data analysis. As prior studies have already demonstrated the performance of kV-based PCA motion modeling techniques using clinical patient images, we believe the results of this analysis will generalize to clinically acquired imaging data.

It is important to note that the XCAT phantoms used in this study are derived from tumor motion observed in patients using orthogonal imaging of implanted fiducial markers during radiotherapy treatments. Consequently, the respiratory motion patterns observed (rate, amplitude, variability) are true representations of the types of respiratory motions that can occur during clinical treatments. Furthermore, the external surrogate signal used for generating the correlation model was also recorded during treatment (not derived from the XCAT phantoms). This means that results presented in this work include any changes in internal-external correlation.

The method presented in this work relies on a motion model built using DVFs generated from DIR between phases of a pre-treatment planning image set. Any uncertainties in these vector fields will be reflected in the motion model, and thus the accuracy of the DIR method places a limit on the precision of the generated images. Although a demons algorithm [69] was used in this work, the method presented could be based on any DIR technique. Using registration techniques that may more accurately incorporate the biomechanical properties of respiratory motion may lead to better results [94,95]. Incorporating models developed from pre-treatment 4DCBCT [25] rather than a planning 4DCT may also improve the accuracy of the method by compensating for day-to-day changes in patient respiratory motion that may differ from the planning 4DCT model during treatment. Compensating for the changes in internal patient anatomy motion that occurs between the time of planning and the time of treatment could also be done by using subpopulation-based correspondence modeling [96]. Moreover, some techniques have been proposed to model respiratory motion without 4DCT images obtained prior to treatment, which could further reduce the dose delivered to the patient in a clinical context [97,98].

This work uses a basic linear correlation model, and although the results (RMSE of 1.47 mm) are in the range expected for SBRT treatments, this technique could potentially be improved by developing a correlation model using a more advanced function or method, such as machine learning, neural networks [99,100], nearest neighbor method [101] or fuzzy logic [41]. Moreover, the linear correlation model could be adjusted after every kV image acquisition. (at every 3 s) so that the continuous correlation model generated PCA weights are forced to agree with the periodic kV image derived PCA weights.

The maximum clinically available in-treatment imaging rate on treatment machines at our institution is set at 1 kV image every 3 s. We used this maximum imaging frame rate in this study to assess the feasibility of this technique (and because we routinely use imaging intervals between 3-5 s to monitor motion in our clinical practice). Changing the time interval of kV image acquisition has the potential to impact the accuracy of the correlation model, and we plan to assess and optimize this rate in a future study.

In this study, the correlation model built for each dataset comes from the entire duration of the respiratory trace. However, the correlation between the internal and external anatomy can potentially change with time [36], and implementing a time-adaptive correlation model that only uses a portion of the respiratory trace may improve accuracy. Additional improvements such as including the uncertainty in the FIR generation process within the model fitting will be investigated in future work.

The continuous volumetric images produced with this technique are inherently coregistered, as they are reconstructed by determining a DVF relative to a reference image. The high rate 3D anatomical image generation made possible with this technique allows to calculate accumulated delivered dose during the fraction with more precision, especially if the planning doses were calculated on the average intensity projection image, in which case discrepancies from the original treatment plan will be made apparent. Through this process, underdosage of the target or overdosage of critical structures can be identified, and corrected in subsequent fractions through treatment plan adaptation.

5. Conclusion

We have demonstrated a new technique for continuously generating dynamic volumetric images of patient anatomy using periodic kV imaging in combination with an external respiratory surrogate. The performance of the method was assessed with 10 digital XCAT phantoms that included clinically measured tumor positions and real patient breathing patterns, which enabled a comparison with ground truth tumor positions, demonstrating tumor localization to better than 1.47 mm on average. Correlation model generated volumetric images were reconstructed with a NRMSE of 97.83% compared to the XCAT phantom ground truth volumetric images.

This method is novel in its combination of kV image-based PCA motion modeling with an external respiratory surrogate amplitude and velocity for volumetric anatomical image reconstruction, which inherently include any changes in internal-external correlation. It enables motion modeling to be performed with high time resolution on data that can be acquired on current clinical linear accelerators (and in some cases is already routinely acquired in clinical practice), without additional kV imaging. The three-dimensional images produced using this technique can be used to calculate delivered dose in the presence of respiratory motion for thoracic and abdominal radiotherapy treatments. This will provide an important tool for treatment verification, delivered dose calculation, and adaptive radiotherapy.

Acknowledgments

We would like to thank Dr. Nishioka of the Department of Radiology, NTT Hospital, Japan, Dr. Shirato of the Department of Radiation Medicine, Hokkaido University, Japan, and Dr. Berbeco of the Radiation Oncology Department at the Brigham & Women's Hospital, Harvard Medical School, USA, for sharing the patient tumor position dataset with our group.

This project was supported through a Master Research Agreement with Varian Medical Systems.

References

[1] Keall P, Mageras GS, Balter JM, Emery RS, Forster KM, Jiang SB, Kapatoes JM, Low DA, Murphy MJ, Murray BR, Ramsey CR, van Herk MB, Vedam SS, Wong JW, Yorke E. The management of respiratory motion in radiation oncology report of AAPM task group 76. Med. Phys. 2006;33(10):3874–900. https://doi.org/10.1118/1.2349696. URL: https://aapm.onlinelibrary.wiley.com/doi/abs/10.1118/1.2349696.

[2] Korreman SS. Image-guided radiotherapy and motion management in lung cancer. Br. J. Radiol. 2015;88(1051):20150100. https://doi.org/10.1259/bjr.20150100. pMID: 25955231.https://doi.org/10.1259/bjr.20150100.

[3] Korreman SS. Phys. Med. Biol. 2012;57(23):R161–91. https://doi.org/10.1088/0031-9155/57/23/r161. URL: https://doi.org/10.1088.

[4] Jiang S. Radiotherapy of mobile tumors. Semin. Radiat. Oncol. 2006;16(4):239–48. https://doi.org/10.1016/j.semradonc.2006.04.007. innovative Technologies in Radiation Therapy.http://www.sciencedirect.com/science/article/pii/S1053429606000336.

[5] Vedam SS, Keall PJ, Kini VR, Mostafavi H, Shukla HP, Mohan R. Acquiring a four-dimensional computed tomography dataset using an external respiratory signal. Phys. Med. Biol. 2003;48(1):45. URL:http://stacks.iop.org/0031-9155/48/i=1/a=304.

[6] Hugo GD, Agazaryan N, Solberg TD. The effects of tumor motion on planning and delivery of respiratory-gated IMRT. Med. Phys. 2003;30(6):1052–66. https://doi.org/10.1118/1.1574611. URL:https://aapm.onlinelibrary.wiley.com/doi/abs/10.1118/1.1574611.

[7] Rietzel E, Pan T, Chen GTY. Four-dimensional computed tomography: Image formation and clinical protocol. Med. Phys. 2005;32(4):874–89. https://doi.org/10.1118/1.1869852. URL: https://aapm.onlinelibrary.wiley.com/doi/abs/10.1118/1.1869852.

[8] Pan T. Comparison of helical and cine acquisitions for 4D-CT imaging with multislice CT. Med. Phys. 2005;32(2):627–34. https://doi.org/10.1118/1.1855013. URL: https://aapm.onlinelibrary.wiley.com/doi/abs/10.1118/1.1855013.

[9] St S, James P, Mishra F, Hacker R, Berbeco J Lewis. Quantifying ITV instabilities arising from 4DCT: a simulation study using patient data. Phys. Med. Biol. 2012;57(5):L1.

[10] Sarker J, Chu A, Mui K, Wolfgang J, Hirsch A, Chen G, Sharp G. Variations in tumor size and position due to irregular breathing in 4d-ct: A simulation study. Med. Phys. 2010;37(3):1254–60. https://doi.org/10.1118/1.3298007. URL: https://aapm.onlinelibrary.wiley.com/doi/abs/10.1118/1.3298007.

[11] Cai J, McLawhorn R, Read P, Larner J, Yin F, Benedict S, Sheng K. Effects of breathing variation on gating window internal target volume in respiratory gated radiation therapy. Med. Phys. 2010;37(8):3927–34. https://doi.org/10.1118/1.3457329. URL: https://aapm.onlinelibrary.wiley.com/doi/abs/10.1118/1.3457329.

[12] Cai J, Read P, Sheng K. The effect of respiratory motion variability and tumor size on the accuracy of average intensity projection from four-dimensional computed tomography: an investigation based on dynamic MRI. Med. Phys. 2008;35(11):4974–81. https://doi.org/10.1118/1.2982245. URL: https://aapm.onlinelibrary.wiley.com/doi/abs/10.1118/1.2982245.

[13] James S St, Seco J, Mishra P, Lewis J. Simulations using patient data to evaluate systematic errors that may occur in 4D treatment planning: a proof of concept study. Med. Phys. 2016;40(9):091706. https://doi.org/10.1118/1.4817244. URL: https://aapm.onlinelibrary.wiley.com/doi/abs/10.1118/1.4817244.

[14] Mishra P, Li R, St S, James R, Mak C, Williams Y, Yue R, Berbeco J Lewis. Evaluation of 3D fluoroscopic image generation from a single planar treatment image on patient data with a modified xcat phantom. Phys. Med. Biol. 2013;58(4):841. https://doi.org/10.1088/0031-9155/58/4/841.

[15] Shieh C-C, Caillet V, Dunbar M, Keall PJ, Booth JT, Hardcastle N, Haddad C, Eade T, Feain I. Phys. Med. Biol. 2017;62(8):3065–80. https://doi.org/10.1088/1361-6560/aa6393. URL: https://doi.org/10.1088.

[16] Fassi A, Schaerer J, Fernandes M, Riboldi M, Sarrut D, Baroni G. Tumor tracking method based on a deformable 4D CT breathing motion model driven by an external surface surrogate. Int. J. Radiat. Oncol.*Biol.*Phys. 2014;88(1):182–8. https://doi.org/10.1016/j.ijrobp.2013.09.026.

[17] Zhang Q, Hu Y, Liu F, Goodman K, Rosenzweig K, Mageras G. Correction of motion artifacts in cone-beam ct using a patient-specific respiratory motion model. Med. Phys. 2010;37(6Part1):2901–9. https://doi.org/10.1118/1.3397460.

[18] Lewis J, Li R, Watkins W, Lawson J, Segars P, Cervino L, Song W, Jiang S. Markerless lung tumor tracking and trajectory reconstruction using rotational cone-beam projections: a feasibility study. Phys. Med. Biol. 2010;55(9):2505. URL: http://stacks.iop.org/0031-9155/55/i=9/a=006.

[19] Zhang Q, Pevsner A, Hertanto A, Hu Y, Rosenzweig K, Ling C, Mageras G. A patient-specific respiratory model of anatomical motion for radiation treatment planning. Med. Phys. 2007;34(12):4772–81. https://doi.org/10.1118/1.2804576. URL: https://aapm.onlinelibrary.wiley.com/doi/abs/10.1118/1.2804576.

[20] Sohn M, Birkner M, Yan D, Alber M. Modelling individual geometric variation based on dominant eigenmodes of organ deformation: implementation and evaluation. Phys. Med. Biol. 2005;50(24):5893. URL: http://stacks.iop.org/0031-9155/50/i=24/a=009.

[21] Hertanto A, Zhang Q, Hu Y, Dzyubak O, Rimner A, Mageras G. Reduction of irregular breathing artifacts in respiration-correlated ct images using a respiratory motion model. Med. Phys. 2012;39(6Part1):3070–9. https://doi.org/10.1118/1.4711802.

[22] Li R, Lewis J, Jia X, Zhao T, Liu W, Wuenschel S, Lamb J, Yang D, Low D, Jiang S. On a PCA-based lung motion model. Phys. Med. Biol. 2011;56(18):6009. URL: http://stacks.iop.org/0031-9155/56/i=18/a=015.

[23] Low DA, Parikh PJ, Lu W, Dempsey JF, Wahab SH, Hubenschmidt JP, Nystrom MM, Handoko M, Bradley JD. Novel breathing motion model for radiotherapy. Int. J. Radiat. Oncol.*Biol.*Phys. 2005;63(3):921–9. https://doi.org/10.1016/j.ijrobp.2005.03.070. URL: http://www.sciencedirect.com/science/article/pii/S036030160500711X.

[24] Cai W, Hurwitz M, Williams C, Dhou S, Berbeco R, Seco J, Mishra P, Lewis J. 3D delivered dose assessment using a 4DCT-based motion model. Med. Phys. 2015;42(6Part1):2897–907. https://doi.org/10.1118/1.4921041.

[25] Dhou S, Hurwitz M, Mishra P, Cai W, Rottmann J, Li R, Williams C, Wagar M, Berbeco R, Ionascu D, Lewis J. 3d fluoroscopic image estimation using patient-specific 4DCBCT-based motion models. Phys. Med. Biol. 2015;60(9):3807. URL: http://stacks.iop.org/0031-9155/60/i=9/a=3807.

[26] Hurwitz M, Williams C, Mishra P, Rottmann J, Dhou S, Wagar M, Mannarino E, Mak R, Lewis J. Generation of fluoroscopic 3d images with a respiratory motion model based on an external surrogate signal. Phys. Med. Biol. 2015;60(2):521. URL: http://stacks.iop.org/0031-9155/60/i=2/a=521.

[27] McClelland J, Hughes S, Modat M, Qureshi A, Ahmad S, Landau D, Ourselin S, Hawkes D. Inter-fraction variations in respiratory motion models. Phys. Med. Biol. 2011;56(1):251. URL: http://stacks.iop.org/0031-9155/56/i=1/a=015.

[28] Staub D, Docef A, Brock R, Vaman C, Murphy M. 4d cone-beam ct reconstruction using a motion model based on principal component analysis. Med. Phys. 2011;38(12):6697–709. https://doi.org/10.1118/1.3662895. URL: https://aapm.onlinelibrary.wiley.com/doi/abs/10.1118/1.3662895.

[29] Cho B, Suh Y, Dieterich S, Keall P. A monoscopic method for real-time tumour tracking using combined occasional x-ray imaging and continuous respiratory monitoring. Phys. Med. Biol. 2008;53(11):2837. URL: http://stacks.iop.org/0031-9155/53/i=11/a=006.

[30] Harris W, Wang C, Yin F, Cai J, Ren L. A novel method to generate on-board 4D MRI using prior 4D MRI and on-board KV projections from a conventional linac for target localization in liver SBRT. Med. Phys. 2018;45(7):3238–45. https://doi.org/10.1002/mp.12998. URL: https://aapm.onlinelibrary.wiley.com/doi/abs/10.1002/mp.12998.

[31] Mishra P, Li R, Mak R, Rottmann J, Bryant J, Williams C, Berbeco R, Lewis J. An initial study on the estimation of time-varying volumetric treatment images and 3D tumor localization from single mv cine epid images. Med. Phys. 2014;41(8Part1):081713. https://doi.org/10.1118/1.4889779. URL: https://aapm.onlinelibrary.wiley.com/doi/abs/10.1118/1.4889779.

[32] Li R, Mok E, Han B, Koong A, Xing L. Evaluation of the geometric accuracy of surrogate-based gated VMAT using intrafraction kilovoltage x-ray images. Med. Phys. 2012;39(5):2686–93. https://doi.org/10.1118/1.4704729. URL: https://aapm.onlinelibrary.wiley.com/doi/abs/10.1118/1.4704729.

[33] Ng JA, Booth J, Poulsen P, Kuncic Z, Keall PJ. Phys. Med. Biol. 2013;58(17):5983–96. https://doi.org/10.1088/0031-9155/58/17/5983. URL: https://doi.org/10.1088.

[34] Crocker JK, Ng JA, Keall PJ, Booth JT. Phys. Med. Biol. 2012;57(10):2969–80. https://doi.org/10.1088/0031-9155/57/10/2969. URL: https://doi.org/10.1088.

[35] Keall PJ, Aun Ng J, O'Brien R, Colvill E, Huang C-Y, Rugaard Poulsen P, Fledelius W, Juneja P, Simpson E, Bell L, Alfieri F, Eade T, Kneebone A, Booth JT. The first clinical treatment with kilovoltage intrafraction monitoring (kim): a real-time image guidance method. Med. Phys. 2015;42(1):354–8. https://doi.org/10.1118/1.4904023.

[36] Wu H, Zhao Q, Berbeco R, Nishioka S, Shirato H, Jiang S. Gating based on internal/external signals with dynamic correlation updates. Phys. Med. Biol. 2008;53(24):7137. URL: http://stacks.iop.org/0031-9155/53/i=24/a=009.

[37] Kanoulas E, Aslam J, Sharp G, Berbeco R, Nishioka S, Shirato H, Jiang S. Derivation of the tumor position from external respiratory surrogates with periodical updating of the internal/external correlation. Phys. Med. Biol. 2007;52(17):5443. URL: http://stacks.iop.org/0031-9155/52/i=17/a=023.

[38] Berbeco RI, Nishioka S, Shirato H, Chen GTY, Jiang SB. Residual motion of lung tumours in gated radiotherapy with external respiratory surrogates. Phys. Med. Biol. 2005;50(16):3655. URL: http://stacks.iop.org/0031-9155/50/i=16/a=001.

[39] Schweikard A, Glosser G, Bodduluri M, Murphy MJ, Adler JR. Robotic motion compensation for respiratory movement during radiosurgery. Comput. Aided Surg. 2000;5(4):263–77. https://doi.org/10.3109/10929080009148894. pMID 11029159.

[40] Yang Z-Y, Chang Y, Liu H-Y, Liu G, Li Q. Target margin design for real-time lung tumor tracking stereotactic body radiation therapy using cyberknife xsight lung tracking system. Sci. Rep. 2017:1–11. https://doi.org/10.1038/s41598-017-11128-w.

[41] Torshabi A, Riboldi M, Fooladi A, Mosalla S, Baroni G. An adaptive fuzzy prediction model for real time tumor tracking in radiotherapy via external surrogates. J. Appl. Clin. Med. Phys. 2013;14(1):102–14. https://doi.org/10.1120/jacmp.v14i1.4008. URL: https://aapm.onlinelibrary.wiley.com/doi/abs/10.1120/jacmp.v14i1.4008.

[42] Collins BT, Erickson K, Reichner CA, Collins SP, Gagnon GJ, Dieterich S, McRae DA, Zhang Y, Yousefi S, Levy E, Chang T, Jamis-Dow C, Banovac F, Anderson ED. Radical stereotactic radiosurgery with real-time tumor motion tracking in the treatment of small peripheral lung tumors. Radiat. Oncol. 2007;2(1):39. https://doi.org/10.1186/1748-717X-2-39.

[43] Sayeh S, Wang J, Main W, Kilby W, Maurer C. Respiratory Motion Tracking for Robotic Radiosurgery. Springer; 2007.

[44] Fu D, Kahn R, Wang B, Wang H, Mu Z, Park J, Kuduvalli G, Maurer C. Xsight Lung Tracking System: A Fiducial-Less Method for Respiratory Motion Tracking. Springer; 2007.

[45] Kilby W, Dooley J, Kuduvalli G, Sayeh S, Maurer C. The cyberknife robotic radiosurgery system in 2010, Technology in Cancer. Res. Treatment 2010;9(5):433–52. https://doi.org/10.1177/153303461000900502. pMID: 20815415.

[46] Kubo HD, Len PM, Minohara S-I, Mostafavi H. Breathing-synchronized radiotherapy program at the university of california davis cancer center. Med. Phys. 2000;27(2):346–53. https://doi.org/10.1118/1.598837. URL: https://aapm.onlinelibrary.wiley.com/doi/abs/10.1118/1.598837.

[47] Ford E, Mageras G, Yorke E, Rosenzweig K, Wagman R, Ling C. Evaluation of

respiratory movement during gated radiotherapy using film and electronic portal imaging. Int. J. Radiat. Oncol.*Biol.*Phys. 2002;52(2):522–31. https://doi.org/10.1016/S0360-3016(01)02681-5.
[48] Wagman R, Yorke E, Ford E, Giraud P, Mageras G, Minsky B, Rosenzweig K. Respiratory gating for liver tumors: use in dose escalation. Int. J. Radiat. Oncol.*Biol.*Phys. 2003;55(3):659–68. https://doi.org/10.1016/S0360-3016(02)03941-X.
[49] Keall P. 4-dimensional computed tomography imaging and treatment planning. Semin. Radiat. Oncol. 2004;14(1):81–90. https://doi.org/10.1053/j.semradonc.2003.10.006. high-Precision Radiation Therapy of Moving Targets.http://www.sciencedirect.com/science/article/pii/S1053429603000870.
[50] Giraud P, Simon L, Saliou M, Reboul F, Garcia R, Carrie C, Lerolle U, Rosenwald JC, Cosset JM. Respiratory gated radiotherapy: the 4D radiotherapy. Bull Cancer 2005;92(1):83–9.
[51] Giraud P, Garcia R. Respiratory gating for radiotherapy: main technical aspects and clinical benefits. Bull Cancer 2010;97(7):847–56.
[52] Low DA, Nystrom M, Kalinin E, Parikh P, Dempsey JF, Bradley JD, Mutic S, Wahab SH, Islam T, Christensen G, Politte DG, Whiting BR. A method for the reconstruction of four-dimensional synchronized ct scans acquired during free breathing. Med. Phys. 2003;30(6):1254–63. https://doi.org/10.1118/1.1576230. URL: https://aapm.onlinelibrary.wiley.com/doi/abs/10.1118/1.1576230.
[53] Zhang T, Jeraj R, Keller H, Lu W, Olivera GH, McNutt TR, Mackie TR, Paliwal B. Treatment plan optimization incorporating respiratory motion. Med. Phys. 2004;31(6):1576–86. https://doi.org/10.1118/1.1739672. URL: https://aapm.onlinelibrary.wiley.com/doi/abs/10.1118/1.1739672.
[54] Zhang T, Keller H, O'Brien MJ, Mackie TR, Paliwal B. Application of the spirometer in respiratory gated radiotherapy. Med. Phys. 2003;30(12):3165–71. https://doi.org/10.1118/1.1625439. URL: https://aapm.onlinelibrary.wiley.com/doi/abs/10.1118/1.1625439.
[55] Zhang T, Keller H, Jeraj R, Manon R, Welsh J, Patel R, Fenwick J, Mehta M, Mackie T, Paliwal B. Breathing synchronized delivery – a new technique for radiation treatment of the targets with respiratory motion. Int. J. Radiat. Oncol.*Biol.*Phys. 2003;57(2 Supplement):S185–6. https://doi.org/10.1016/S0360-3016(03)00980-5. URL: http://www.sciencedirect.com/science/article/pii/S0360301603009805.
[56] Segars P, Sturgeon G, Mendonca S, Grimes J, Tsui B. 4D XCAT phantom for multimodality imaging research. Med. Phys. 2010;37(9):4902–15. https://doi.org/10.1118/1.3480985. URL: https://aapm.onlinelibrary.wiley.com/doi/abs/10.1118/1.3480985.
[57] Segars P, Tsui B, Lalush D, Frey E, King M, Manocha D. Development and application of the new dynamic nurbs-based cardiac-torso (NCAT) phantom. J. Nucl. Med. 2001;42:23.
[58] Segars P, Lalush D, Tsui B. Modeling respiratory mechanics in the MCAT and spline-based MCAT phantoms. IEEE Trans. Nucl. Sci. 2001;48(1):89–97. https://doi.org/10.1109/23.910837.
[59] Spitzer V, Whitlock D. The visible human dataset: the anatomical platform for human simulation. Anat. Rec. 1998;253(2):49–57. https://doi.org/10.1002/(SICI)1097-0185(199804)253:2<49::AID-AR8>3.0.CO;2-9.
[60] Berbeco RI, Mostafavi H, Sharp GC, Jiang SB. Towards fluoroscopic respiratory gating for lung tumours without radiopaque markers. Phys. Med. Biol. 2005;50(19):4481. URL: http://stacks.iop.org/0031-9155/50/i=19/a=004.
[61] Pankaj M, St S, James P, Segars R, Berbeco J Lewis. Adaptation and applications of a realistic digital phantom based on patient lung tumor trajectories. Phys. Med. Biol. 2012;57(11):3597.
[62] Cai W, Dhou S, Cifter F, Myronakis M, Hurwitz M, Williams C, Berbeco R, Seco J, Lewis J. 4d cone beam ct-based dose assessment for SBRT lung cancer treatment. Phys. Med. Biol. 2016;61(2):554. URL: http://stacks.iop.org/0031-9155/61/i=2/a=554.
[63] Williams C, Mishra P, Seco J, James S St, Mak R, Berbeco R, Lewis J. A mass-conserving 4D XCAT phantom for dose calculation and accumulation. Med. Phys. 2013;40(7):071728. https://doi.org/10.1118/1.4811102. URL: https://aapm.onlinelibrary.wiley.com/doi/abs/10.1118/1.4811102.
[64] Shirato H, Shimizu S, Kitamura K, Nishioka T, Kagei K, Hashimoto S, Aoyama H, Kunieda T, Shinohara N, Dosaka-Akita H, Miyasaka K. Four-dimensional treatment planning and fluoroscopic real-time tumor tracking radiotherapy for moving tumor. Int. J. Radiat. Oncol.*Biol.*Phys. 2000;48(2):435–42. https://doi.org/10.1016/S0360-3016(00)00625-8.
[65] Shirato H, Shimizu S, Kunieda T, Kitamura K, van Herk M, Kagei K, Nishioka T, Hashimoto S, Fujita K, Aoyama H, Tsuchiya K, Kudo K, Miyasaka K. Physical aspects of a real-time tumor-tracking system for gated radiotherapy. Int. J. Radiat. Oncol.*Biol.*Phys. 2000;48(4):1187–95. https://doi.org/10.1016/S0360-3016(00)00748-3.
[66] Berbeco RI, Nishioka S, Shirato H. Evaluation of the need for simultaneous orthogonal gated setup imaging. J. Appl. Clin. Med. Phys. 2010;11(2):158–67. https://doi.org/10.1120/jacmp.v11i2.3203. URL: https://aapm.onlinelibrary.wiley.com/doi/abs/10.1120/jacmp.v11i2.3203.
[67] Myronakis M, Cai W, Dhou S, Cifter F, Hurwitz M, Segars P, Berbeco R, Lewis J. A graphical user interface for XCAT phantom configuration, generation and processing. Biomed. Phys. Eng. Express 2017;3(1):017003. URL: http://stacks.iop.org/2057-1976/3/i=1/a=017003.
[68] Li R, Lewis J, Jia X, Gu X, Folkerts M, Men C, Song W, Jiang S. 3d tumor localization through real-time volumetric x-ray imaging for lung cancer radiotherapy. Med. Phys. 2011;38(5):2783–94. https://doi.org/10.1118/1.3582693. URL: https://aapm.onlinelibrary.wiley.com/doi/abs/10.1118/1.3582693.
[69] Gu X, Pan H, Liang Y, Castillo R, Yang D, Choi D, Castillo E, Majumdar A, Guerrero T, Jiang S. Implementation and evaluation of various demons deformable image registration algorithms on a GPU. Phys. Med. Biol. 2010;55(1):207. URL: http://stacks.iop.org/0031-9155/55/i=1/a=012.
[70] Zhang Y, Yang J, Zhang L, Court L, Balter P, Dong L. Modeling respiratory motion for reducing motion artifacts in 4D CT images. Med. Phys. 2013;40(4):041716https://doi.org/10.1118/1.4795133. URL: https://aapm.onlinelibrary.wiley.com/doi/abs/10.1118/1.4795133.
[71] Li R, Jia X, Lewis J, Gu X, Folkerts M, Men C, Jiang S. Real-time volumetric image reconstruction and 3d tumor localization based on a single X-ray projection image for lung cancer radiotherapy. Med. Phys. 2010;37(6Part1):2822–6. https://doi.org/10.1118/1.3426002.
[72] Vaman C, Staub D, Williamson J, Murphy M. A method to map errors in the deformable registration of 4DCT images. Med. Phys. 2010;37(11):5765–76. https://doi.org/10.1118/1.3488983. URL: https://aapm.onlinelibrary.wiley.com/doi/abs/10.1118/1.3488983.
[73] Zeng R, Fessler JA, Balter J. Estimating 3-D respiratory motion from orbiting views by tomographic image registration. IEEE Trans. Med. Imaging 2007;26(2):153–63. https://doi.org/10.1109/TMI.2006.889719.
[74] Zhao T, Lu W, Yang D, Mutic S, Noel C, Parikh P, Bradley J, Low D. Characterization of free breathing patterns with 5d lung motion model. Med. Phys. 2009;36(11):5183–9. https://doi.org/10.1118/1.3246348. URL: https://aapm.onlinelibrary.wiley.com/doi/abs/10.1118/1.3246348.
[75] Keall PJ, Nguyen DT, O'Brien R, Caillet V, Hewson E, Poulsen PR, Bromley R, Bell L, Eade T, Kneebone A, Martin J, Booth JT. The first clinical implementation of real-time image-guided adaptive radiotherapy using a standard linear accelerator. Radiother. Oncol. 2018;127(1):6–11. https://doi.org/10.1016/j.radonc.2018.01.001. URL: http://www.sciencedirect.com/science/article/pii/S0167814018300161.
[76] Keall PJ, Nguyen DT, O'Brien R, Zhang P, Happersett L, Bertholet J, Poulsen PR. Review of real-time 3-dimensional image guided radiation therapy on standard-equipped cancer radiation therapy systems: are we at the tipping point for the era of real-time radiation therapy? Int. J. Radiat. Oncol.*Biol.*Phys. 2018;102(4):922–31. https://doi.org/10.1016/j.ijrobp.2018.04.016. imaging in Radiation Oncology.http://www.sciencedirect.com/science/article/pii/S0360301618306680.
[77] Zhang P, Hunt M, Telles AB, Pham H, Lovelock M, Yorke E, Li G, Happersett L, Rimner A, Mageras G. Design and validation of a mv/kv imaging-based markerless tracking system for assessing real-time lung tumor motion. Med. Phys. 2018;45(12):5555–63. https://doi.org/10.1002/mp.13259. URL: https://aapm.onlinelibrary.wiley.com/doi/abs/10.1002/mp.13259.
[78] Nguyen DT, O'Brien R, Kim J-H, Huang C-Y, Wilton L, Greer P, Legge K, Booth JT, Poulsen PR, Martin J, Keall PJ. The first clinical implementation of a real-time six degree of freedom target tracking system during radiation therapy based on kilovoltage intrafraction monitoring (kim). Radiother. Oncol. 2017;123(1):37–42. https://doi.org/10.1016/j.radonc.2017.02.013. URL: http://www.sciencedirect.com/science/article/pii/S0167814017300907.
[79] Keall P, Nguyen DT, O'Brien R, Booth J, Greer P, Poulsen P, Gebski V, Kneebone A, Martin J. Stereotactic prostate adaptive radiotherapy utilising kilovoltage intrafraction monitoring: the trog 15.01 spark trial. BMC Cancer 2017;17(1):180. https://doi.org/10.1186/s12885-017-3164-1.
[80] Colvill E, Booth J, Nill S, Fast M, Bedford J, Oelfke U, Nakamura M, Poulsen P, Worm E, Hansen R, Ravkilde T, Rydhg JS, Pommer T, af Rosenschold PM, Lang S, Guckenberger M, Groh C, Herrmann C, Verellen D, Poels K, Wang L, Hadsell M, Sothmann T, Blanck O, Keall P. A dosimetric comparison of real-time adaptive and non-adaptive radiotherapy: a multi-institutional study encompassing robotic, gimbaled, multileaf collimator and couch tracking. Radiother. Oncol. 119(1), 2016,:159–65. https://doi.org/10.1016/j.radonc.2016.03.006.
[81] Cho B, Poulsen PR, Sawant A, Ruan D, Keall PJ. Real-time target position estimation using stereoscopic kilovoltage/megavoltage imaging and external respiratory monitoring for dynamic multileaf collimator tracking. Int. J. Radiat. Oncol.*Biol.*Phys. 2011;79(1):269–78. https://doi.org/10.1016/j.ijrobp.2010.02.052.
[82] Xing L, Siebers J, Keall P. Computational challenges for image-guided radiation therapy: Framework and current research. Semin. Radiat. Oncol. 2007;17(4):245–57. https://doi.org/10.1016/j.semradonc.2007.07.004. image-Guided Radiation Therapy.http://www.sciencedirect.com/science/article/pii/S1053429607000616.
[83] He P, Li Q, Xiao G, Wang X, Ouyang S, Liu R. Effect of respiratory guidance on internal/external respiratory motion correlation for synchrotron-based pulsed heavy-ion radiotherapy. Austral. Phys. Eng. Sci. Med. 2018;41(3):713–20. https://doi.org/10.1007/s13246-018-0667-2.
[84] Wu H, Besemer A, Lu M. Dynamic correlation of synchronized internal tumor and external skin respiratory motion for image guided lung cancer radiation treatment. Int. J. Comput. Appl. 2014;21(1):14–23.
[85] Fayad H, Pan T, Clement J, Visvikis D. Technical note: correlation of respiratory motion between external patient surface and internal anatomical landmarks. Med. Phys. 2011;38(6Part1):3157–64. https://doi.org/10.1118/1.3589131.
[86] Liu C, Alessio A, Kinahan P. Respiratory motion correction for pet/ct with internal-external motion correlation. J. Nucl. Med. 2010;51(supplement 2):78. URL: http://jnm.snmjournals.org/content/51/supplement_2/78.abstract.
[87] Nishioka S, Nishioka T, Kawahara M, Tanaka S, Hiromura T, Tomita K, Shirato H. Exhale fluctuation in respiratory-gated radiotherapy of the lung: a pitfall of respiratory gating shown in a synchronized internal/external marker recording study. Radiother. Oncol. 2008;86(1):69–76. https://doi.org/10.1016/j.radonc.2007.11.014. URL: http://www.sciencedirect.com/science/article/pii/S0167814007005646.
[88] Beddar AS, Kainz K, Briere TM, Tsunashima Y, Pan T, Prado K, Mohan R, Gillin M, Krishnan S. Correlation between internal fiducial tumor motion and external

marker motion for liver tumors imaged with 4d-ct. Int. J. Radiat. Oncol.*Biol.*Phys. 2007;67(2):630–8. https://doi.org/10.1016/j.ijrobp.2006.10.007.

[89] Ionascu D, Jiang S, Nishioka S, Shirato H, Berbeco R. Internal-external correlation investigations of respiratory induced motion of lung tumors. Med. Phys. 2007;34(10):3893–903. https://doi.org/10.1118/1.2779941. URL: https://aapm.onlinelibrary.wiley.com/doi/abs/10.1118/1.2779941.

[90] Korreman S, Mostafavi H, Le Q-T, Boyer A. Comparison of respiratory surrogates for gated lung radiotherapy without internal fiducials. Acta Oncol. 2006;45(7):935–42. https://doi.org/10.1080/02841860600917161.

[91] Gierga D, Brewer J, Sharp G, Betke M, Willett C, Chen G. The correlation between internal and external markers for abdominal tumors: Implications for respiratory gating. Int. J. Radiat. Oncol.*Biol.*Phys. 2005;61(5):1551–8. https://doi.org/10.1016/j.ijrobp.2004.12.013. URL: http://www.sciencedirect.com/science/article/pii/S0360301604030391.

[92] Rubio C, Morera R, Hernando O, Leroy T, Lartigau S. Extracranial stereotactic body radiotherapy review of main sbrt features and indications in primary tumors. Rep. Practical Oncol. Radiother. 2013;18(6):387–96. https://doi.org/10.1016/j.rpor.2013.09.009. selected Papers Presented at the XVII SEOR Congress, Vigo, 18–21 June 2013.http://www.sciencedirect.com/science/article/pii/S1507136713010596.

[93] Hoogeman M, Prvost J-B, Nuyttens J, Pll J, Levendag P, Heijmen B. Clinical accuracy of the respiratory tumor tracking system of the cyberknife: assessment by analysis of log files. Int. J. Radiat. Oncol.*Biol.*Phys. 2009;74(1):297–303. https://doi.org/10.1016/j.ijrobp.2008.12.041.

[94] Samavati N, Velec M, Brock K. A hybrid biomechanical intensity based deformable image registration of lung 4DCT. Phys. Med. Biol. 2015;60(8):3359. URL: http://stacks.iop.org/0031-9155/60/i=8/a=3359.

[95] Brock K. Results of a multi-institution deformable registration accuracy study (midras). Int. J. Radiat. Oncol.*Biol.*Phys. 2010;76(2):583–96. https://doi.org/10.1016/j.ijrobp.2009.06.031.

[96] Wilms M, Werner R, Yamamoto T, Handels H, Ehrhardt J. Phys. Med. Biol. 2017;62(14):5823–39. https://doi.org/10.1088/1361-6560/aa70cc. URL: https://doi.org/10.1088.

[97] Fayad H, Gilles M, Pan T, Visvikis D. A 4D global respiratory motion model of the thorax based on ct images: a proof of concept. Med. Phys. 2018;45(7):3043–51. https://doi.org/10.1002/mp.12982. URL: https://aapm.onlinelibrary.wiley.com/doi/abs/10.1002/mp.12982.

[98] McClelland JR, Modat M, Arridge S, Grimes H, D'Souza D, Thomas D, Connell DO, Low DA, Kaza E, Collins DJ, Leach MO, Hawkes DJ. Phys. Med. Biol. 2017;62(11):4273–92. https://doi.org/10.1088/1361-6560/aa6070. URL: https://doi.org/10.1088.

[99] Seregni M, Pella A, Riboldi M, Orecchia R, Cerveri P, Baroni G. Real-time tumor tracking with an artificial neural networks-based method: a feasibility study. Phys. Med. 2013;29(1):48–59. https://doi.org/10.1016/j.ejmp.2011.11.005. URL: http://www.sciencedirect.com/science/article/pii/S1120179711001426.

[100] Isaksson M, Jalden J, Murphy M. On using an adaptive neural network to predict lung tumor motion during respiration for radiotherapy applications. Med. Phys. 2005;32(12):3801–9. https://doi.org/10.1118/1.2134958. URL: https://aapm.onlinelibrary.wiley.com/doi/abs/10.1118/1.2134958.

[101] Zhang J, Huang X, Shen Y, Chen Y, Cai J, Ge Y. Nearest neighbor method to estimate internal target for real-time tumor tracking. Technol. Cancer Res. Treat. 2018;17. https://doi.org/10.1177/1533033818786597. pMID: 30081745.https://doi.org/10.1177/1533033818786597.